Phase transition kinetics in Langmuir and spin-coated polydiacetylene films†

Yevgeniy Lifshitz,‡[a] Alexander Upcher,‡[a] Olga Shusterman,[c] Baruch Horovitz,[c] Amir Berman*[b] and Yuval Golan*[a]

Received 3rd August 2009, Accepted 21st October 2009
First published as an Advance Article on the web 19th November 2009
DOI: 10.1039/b915527a

Thin films of 10,12-pentacosadiynoic acid were prepared using Langmuir and spin-coating techniques and polymerized using a controlled dosage of UV radiation. The radiation-induced phase transitions: from the colorless monomer, *via* the metastable blue phase, to the red polydiacetylene phase, and finally to degradation of the material, were monitored by optical absorbance spectroscopy. Deconvolution analysis of the absorbance curves allowed us to monitor quantitatively the dynamical changes in the chromatic properties of the films as a function of applied UV radiation dose. Several reaction kinetics models were applied in order to describe the phase transitions in the films. The results present the phase evolution in PDA and compare the kinetics for Langmuir films *vs.* spin-coated films. Polymerization directly at the air–water interface was found to be two-to-three orders of magnitude faster compared to solid-supported films of the same material. Moreover, we show that the data of the solid supported films is considerably better fitted when a reversible intermediate phase between the blue and the red phases is considered. Furthermore, a shift of the Raman active triple bond supports the presence of the intermediate phase.

Introduction

Size and morphology dependent physical properties which differentiate molecularly thick films from the bulk are of immense fundamental and technological interest. Appearing in different physical shapes to vesicles,[1–3] self-assembled monolayers[4] and Langmuir films (LF),[5] diacetylene derivatives constitute the active part of long and often complicated molecules or structures.[4] The chromatic properties of polydiacetylenes (PDA) have been widely studied[6–8] and were recently described.[9] In general, the colorless monomer transforms into the metastable blue phase and then to its final red phase state. The initial polymerization (Scheme 1) can be initiated by UV, X-ray or gamma irradiation, or by a visible light 2-photon process,[10] whereas the transition from blue to red can be activated by radiation, by biological recognition,[11] chemically, or mechanically.[12] The blue to red chromatic transition (***B*** → ***R***) is complicated and apparently comprised of several stages which normally include rearrangement of the alkyl side chains.[9,13–15] In one possible scenario, an intermediate, so-called "purple phase" was identified with characteristic Raman and optical absorbance peaks located in between the common blue and red peaks.[9,13,16,17] The chromatic transition kinetics of PDA are highly sensitive to factors such as temperature,[17–19] surface pressure,[20] substrate[21] and subphase composition.[17] Understanding the effect of these factors on the phase transitions is key for sensing and detection applications of PDA.[22] These applications include detection of biological species such as microorganisms, viruses and proteins,[23] biosensors on the basis of a surface host–guest recognition process,[24] and colorimetric sensors for drug discovery and biomedical diagnostics.[25] Chromatic changes in PDA have been typically described in terms of a qualitative color change of vesicle solutions or films by the so-called "colorimetric response".[4,18,25,26] However, only few studies have treated the chromatic transition properties of PDA in a quantitative manner. First-order reaction kinetics analysis was successfully adapted to describe the phase transitions of PDA LF from the colorless monomer, *via* the metastable blue, to the final red phases (***M*** → ***B*** → ***R***) based on optical absorbance.[19,27] It was also showed that prolonged irradiation of diacetylenes resulted in degradation of the polymer due to photo-oxidation reactions.[28] The post-polymerization degradation of PDA LB films was studied by Raman spectroscopy.[29]

In this work we present a quantitative optical absorbance study of PDA films prepared by two different techniques: (i) Langmuir deposition, in which molecularly thick films were prepared in a highly controlled manner by spreading and compressing 10,12-pentacoasdiynoic acid (PCDA) monomers at the air–water interface, and (ii) the spin-coating technique (SC), in which PCDA monomers dissolved in an appropriate solvent are placed on a spinning solid support, followed by solvent evaporation. For the PDA Langmuir films two types

[a] *Materials Engineering Department and Ilse Katz Center of Nanoscience, Ben Gurion University of the Negev, Beer-Sheva 84105, Israel. E-mail: ygolan@bgu.ac.il*
[b] *Department of Biotechnology Engineering and Ilse Katz Center of Nanoscience, Ben Gurion University of the Negev, Beer-Sheva 84105, Israel. E-mail: aberman@bgu.ac.il*
[c] *Department of Physics and Ilse Katz Center of Nanoscience, Ben Gurion University of the Negev, Beer-Sheva 84105, Israel*
† Electronic supplementary information (ESI) available: AFM images; details of the kinetic model. See DOI: 10.1039/b915527a
‡ Authors who contributed equally to this work.

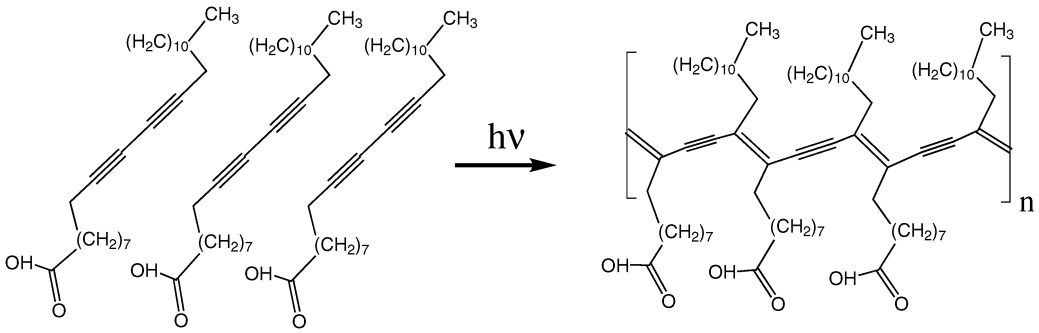

Scheme 1 Topotactic polymerization reaction of diacetylene lipid PCDA.

of production methods were applied. Films that were directly polymerized at the air–water interface and subsequently transferred onto glass slides are denoted LF^W (Langmuir Films polymerized on water), while films deposited onto quartz slides prior to polymerization are defined as LF^S (Langmuir Films polymerized on a solid support).

In all cases, pure PDA films were prepared without any added dopants or additives. Deconvolution of the background-corrected absorbance curves into their constituent Lorenzian shaped peaks allowed to follow the dynamical changes in the chromatic properties of the films, which were correlated with the UV radiation doses applied. The resulting exposure-resolved curves quantitatively describe the evolution of the chromatic phases in PDA and directly compare the polymerization kinetics of films prepared by LF^W, LF^S and SC. Such diagrams are important for understanding the potential of PDA as colorimetric sensors and can be in principle applied to other useful materials systems in which the absorbance spectrum is highly sensitive to external factors.

Results and discussion

Data analysis

The chromatic phase behavior of PDA was monitored by optical absorbance. The PCDA monomer precursor phase does not absorb visible light, and its spectra were not monitored. PDA blue and red phases strongly absorb light in the visible range, and differ significantly from each other. A typical evolution of the absorbance spectra of Langmuir and SC polydiacetylene films as a function of increasing dose of UV radiation is shown in Fig. 1. A prominent observation is that each spectrum consists of different ratios of peaks corresponding to the blue and red phases of PDA.

Previous studies have mostly followed the chromatic phase transitions of PDA, using raw optical absorbance spectra, without background subtraction and peak deconvolution. Monitoring of peak heights in unprocessed data does not provide reliable information on the relative phase fraction during the course of phase transformation, primarily due to different background levels and peak convolution that lead to misjudgement of their real intensity. In order to account for this situation, Lorenz deconvolution was applied to the background-corrected absorbance curves, Fig. 2. Consequently, accurate information of peak area, width and center of mass (COM) of the absorbance peaks allows for quantitative monitoring of the evolution of each peak as a function of irradiation. The COM and peak widths refer to the vibrational and excitonic states of each chromatic phase. Typically, the peak widths are *circa* 40 nm for the excitonic peak and 60 nm for the vibronic peak. The combined area of the deconvoluted excitonic and vibronic peaks is proportional to the fraction of photons that are absorbed either in blue or red PDA structures, allowing for monitoring of the fraction of each phase. We assume the same extinction coefficient for the blue and red phases, since the maximal absorbance value for both of the chromatic phases are almost equal for the SC and LF^S films. According to our models and fits to the data, LF^W does not show this due to the faster kinetics of the blue to red transition, leading to a small proportion of the blue phase within the film. (*v.i.* in Fig. 4).

For all PDA film types, the entire polymerization process was divided into three characteristic regions. The start and the end of each stage are marked with black solid and dashed lines, respectively. The spectra were deconvoluted in the subsequent stage of data processing. The deconvolution of the spectra presented in green (bold lines) are depicted in detail in Fig. 2. For the initial stage of polymerization (Stage I; Fig. 1a, d and g, solid lines) the first absorbance spectrum obtained for each film type is characteristic of a monomer film. Hence, no characteristic peaks were observed in the visible spectrum. According to our interpretation, the intensity of the background level of the absorbance curve at this stage scales with film thickness. Indeed, the absorbance obtained for SC films is indeed 4–5 times greater than for LFs.

During the first part of the polymerization process (Stage I) the peaks associated with the blue phase reach their maximum. For the SC films, the initial (blue phase) COM of the excitonic and vibronic peaks are at 660 nm and 610 nm, respectively. During the evolution of the blue phase the COM of the excitonic peak shifts to 640 nm and the vibronic to 590 nm, with a simultaneous increase in intensity (Fig. 1a and 2a). Interestingly, these peaks relax back to the initial positions of 660 nm and 610 nm upon further radiation exposure at intermediate UV doses (Fig. 1b and 2b).

PCDA Langmuir films polymerized on quartz substrate with hydrophobic or hydrophilic interactions between molecules and solid supports (see the Experimental section) showed no difference and are therefore considered the same and denoted LF^S. At low UV doses LF^S, blue vibronic and

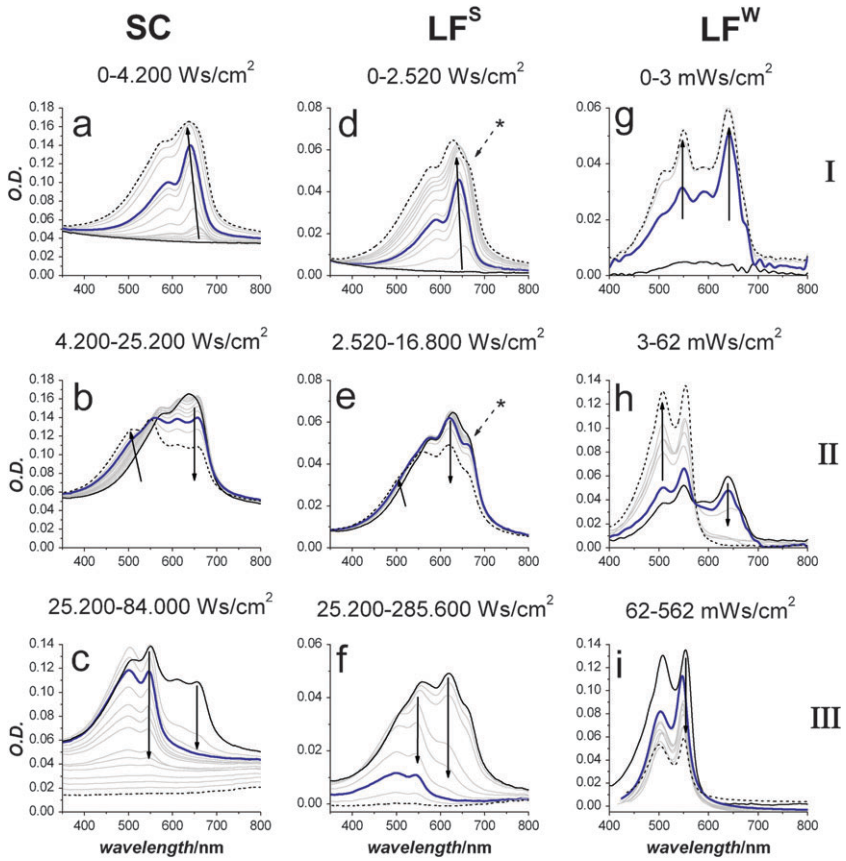

Fig. 1 Evolution of optical absorbance spectra with increasing UV irradiation for (a–c) SC films, (d–f) LF^S and (g–i) LF^W. The solid and dashed black lines indicate the initial and final scans at every stage, respectively. The actual curves used for deconvolution in Fig. 2 are marked in bold lines. The arrows show the direction of absorbance spectra evolution with increasing irradiation. The dashed arrows in LF^S indicate the presence of additional spectral features centred at *ca.* 670 nm.

excitonic peaks appear at 595 and 645 nm, respectively. During the evolution of the blue phase both peaks shift to lower wavelengths of 590 and 635 nm (Fig. 1d and 2d).

A slightly different behaviour was observed for LF^W. Due to the much faster polymerization kinetics, a substantial fraction of the blue phase could not be reached and transition to the red phase starts before polymerization of the blue phase is completed, even at low UV doses. Throughout the evolution of the blue phase in LF^W, the positions of the COM remained constant at 590 nm and 640 nm for the vibronic and excitonic peaks, respectively (Fig. 1g and 2g).

During Stage II of PDA irradiation (Fig. 2b, e and h) the film changes its color from blue to red, manifested in changes of the absorbance spectrum. Initially, the excitonic and vibronic red phase peaks in SC and LF^S appear at 570 nm and 530 nm, respectively. Then, during the intermediate irradiation stage the COM of those peaks shifts to 550 nm and 500 nm, respectively (Fig. 1b, e and 2b, e). Another unique absorption peak is associated with the blue phase is centred at 670 nm appears exclusively in LF^S at intermediate UV doses (marked "*" in Fig. 2e). In SC films, the 670 nm absorption peak is not observed although polymerization was also carried out on solid substrate. The same absorption peak was also observed in PDA LF^W produced on the Zn^{2+} containing subphase, where the chromatic phase transition occurs at a much slower rate than on pure water.[30] For LF^W, the COM of the red phase characteristic peaks remains constant upon irradiation (500 nm to 550 nm) (Fig. 1h).

Our Raman measurements, obtained with a 633 nm excitation laser, for the SC film during Stages I and II of the irradiation process show a triple bond of carbon stretching frequencies. We observe that there is a shift from higher frequency of 2101 cm^{-1} to lower frequency of 2080 cm^{-1} during the UV irradiation (Fig. 3a and b). In the inset of Fig. 3a we show the same shift as observed by a 788 nm laser. In this case the polymerization proceeds *via* the laser itself (*i.e.* UV is not applied); polymerization is a 2-photon process.[10] We note that here the coexistence of two peaks is resolved, consistent with a phase separation.

In the final stage of the polymerization process the $\boldsymbol{B} \rightarrow \boldsymbol{R}$ transition is completed, and as a result, at high UV doses only the red phase is present (Stage III; Fig. 2c, f and i). The prolonged exposure of the films to UV irradiation results in eventual film degradation. Film degradation proceeds by cleavage of carbon–carbon bonds, typically by a photo-oxidation reaction.[28] Consequently, two observations can be noted in the absorbance spectrum: (i) loss of the absorbance signal in the visible range due to decomposition of the polymer, and (ii) a decrease in background intensity (Fig. 1c, f and i). Interestingly, at high UV dose the background level is lower

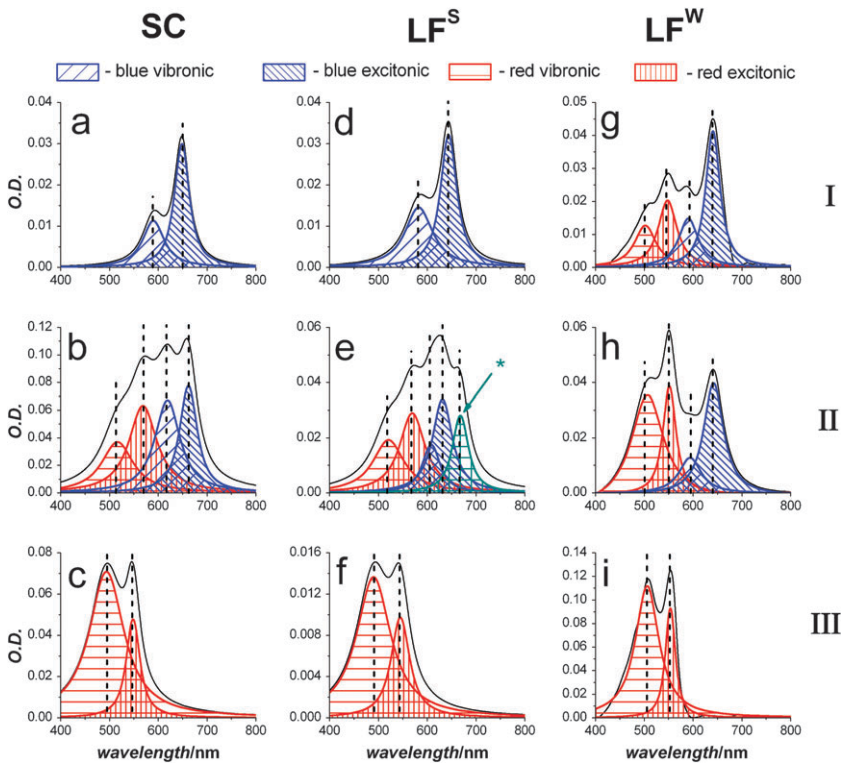

Fig. 2 Deconvolution of background-subtracted absorbance spectra of (a–c) SC films, (d–f) LF^S and (g–i) LF^W with increasing UV exposure. The thick black curves highlight the experimental data. The deconvoluted peaks correspond to the excitonic and vibronic states of the blue and red phases, respectively. Note the additional absorbance peak observed for LF^S at 670 nm. The dashed lines define the COM positions of the deconvoluted absorbance peaks.

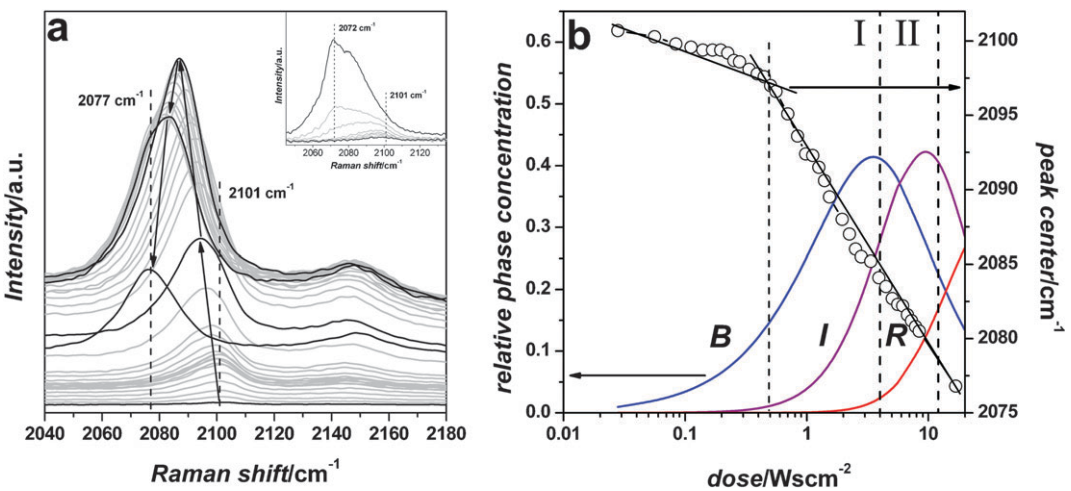

Fig. 3 (a) Raman spectra of the SC sample, excited with 633 nm laser, showing the evolution of the carbon triple bond stretching frequency with increasing dose of UV irradiation. The irradiation range was between 0–16.8 W s cm^{-2}. The arrows show shifting of the peak center during the evolution, while spectra marked with the black lines represent the meaningful stages throughout this process. Note that the red phase triple bond frequency is centred *circa* 2120 cm^{-1}, hence the Raman shift is not related to the red phase. The inset shows Raman spectra evolution of the carbon stretching triple bond frequency excited with a 788 nm laser; polymerization proceeds in this case by the laser itself. (b) Shifting of the triple bond frequency peak center for 633 nm excitation laser and the relative phase fraction calculated from the reversible kinetic model (RKM), eqn (11) *vs.* dose of UV irradiation. Note the good correlation between triple bond peak shifting and the appearance of the intermediate phase (***I***).

than in the monomer spectrum, indicating degradation of the polymer film. This is supported by the AFM images in Figure S1 (ESI†), which clearly show the disappearance of the film from the solid quartz substrate at high irradiation doses.

Modelling of PDA reaction kinetics

Monomer → polymer → degradation transition

Simple kinetic model (SKM). A first order reaction kinetics model was used in order to describe the phase transition of

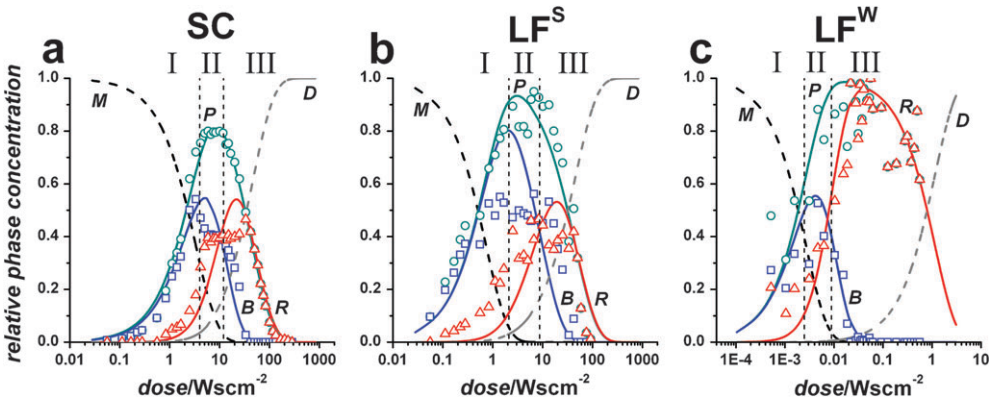

Fig. 4 Exposure-resolved plots calculated based on the unidirectional kinetic model (eqn (5)) depicting the phase transitions of PDA for (a) SC films, (b) LF^S and (c) LF^W. The empty squares, triangles and circles represent experimental data for the blue, red and polymer phases, respectively. The (***P***), (***B***) and (***R***) solid lines are fits calculated from eqn (6)–(9) allowed us to estimate the values of the kinetic constants, k_1, k_2 and k_5. Note the very different log scales of the *x*-axis in (a, b) and in (c).

PDA films. SKM model assumes the existence of the following three phases:

M—Monomer phase (the unpolymerized part of the film).

P—Polymer phase (the polymerized part of the film).

D—Degradation phase (the part of the film that was damaged and eventually removed from the substrate).

Two exposure-dependent kinetic constants were defined in order to describe the transformation rate in each stage: k_1 and k_5 $(W\ s\ cm^{-2})^{-1}$, are the rate constants for $\boldsymbol{M} \rightarrow \boldsymbol{P}$ and $\boldsymbol{P} \rightarrow \boldsymbol{D}$ transitions respectively, and are presented by expression (1):

$$\boldsymbol{M} \xrightarrow{k_1} \boldsymbol{P} \xrightarrow{k_5} \boldsymbol{D} \qquad (1)$$

Setting the initial amount of monomer to unity, the fractions of the monomer ***M***, polymer ***P*** and degradation stage ***D*** as a function of radiation exposure, H, $(W\ s\ cm^{-2})$ can be calculated using eqn (2)–(4):

$$\frac{d\boldsymbol{M}}{d\boldsymbol{H}} = -k_1\boldsymbol{M} \qquad (2)$$

$$\frac{d\boldsymbol{P}}{d\boldsymbol{H}} = k_1\boldsymbol{M} - k_5\boldsymbol{P} \qquad (3)$$

$$\frac{d\boldsymbol{D}}{d\boldsymbol{H}} = k_5\boldsymbol{P} \qquad (4)$$

The films' evolution from monomer ***M*** to polymer ***P*** and finally to degradation stage of the film ***D***, is presented in Fig. 4 (Note that curves (***B***) and (***R***), as well as the empty squares and triangles were derived from the unidirectional kinetic model, which is discussed in detail in the next section). The experimental data was acquired by integration of the optical absorbance signal obtained in the visible spectrum between 400 to 800 nm. The experimental data was then normalized with respect to the maximum value of integrated absorbance of the polymer phase. Fitting the experimental data with the kinetics models presented here requires an additional normalization parameter (polymer contents, *z*) for each film type, which involves the extinction coefficient of the ***B*** and ***R*** phases (assumed equal) and relates the total polymer amount to the normalized absorbance. Note that only the calculated concentration of the monomer and "degradation" phases can be shown, since neither the monomer nor the degradation phases could be measured by optical absorbance.

The kinetic constants obtained by SKM (Table 1) represent the polymerization and degradation rate of the films. Their values and ratio elucidate and compare the kinetic processes within the films. In SC films the polymerization rate is the slowest among all films (k_1 constant). In LF^S the rate of polymerization is one order of magnitude faster than in SC films and two orders of magnitude slower than in LF^W. These differences in rate constants can be explained by the degree of molecular mobility on the substrate. Since the $\boldsymbol{M} \rightarrow \boldsymbol{B}$ transition is a topotactic reaction, the molecules must form a suitable close-packed structure prior to UV irradiation in order for polymerization to take place. The molecular mobility is more facile for monomer films at the air–water interface compared to LF^S and SC films, thus polymerization of LF^W is expected to be faster than solid supported films. Our recent grazing incidence X-ray diffraction and transmission electron microscopy studies have showed that each PDA phase (***M***, ***B*** and ***R***) has its unique crystal structure, and moreover, the phase transition in each polymerization stage is associated with rearrangement of the molecular structure that is manifested in appearance of cleavage planes, cracks and other film defects and associated with alkyl chain straightening.[15] Lateral motion of the monomers and polymerized chains is expected to be more facile on the water subphase *vs.* solid substrate, whereas chain straightening will slow the kinetics in the multilayered SC films and less so in LF^S.

The rate of the polymer degradation is denoted by the k_5 kinetic constant. The degradation rate has the same order of magnitude for both films polymerized on solid substrate, yet it occurs 40 times faster on water, due to the high rate of phase transitions.

Blue → red transition

Unidirectional kinetic model (UKM). The blue to red chromatic phase transition is one of the most attracting features of PDA for its potential as responsive material and a basis for different chemical and biological sensory applications.

Table 1 List of kinetic constants (corresponding to the various chromatic phase transitions of PDA Langmuir and spin-coated films under ambient conditions), normalization parameter (z), distribution parameter (x), and quality of fit parameter (χ^2) between the measured data and best fit for all models. A comparison between all cases is given in order to underline the contribution of reversible kinetic reaction

	k_1/(W s cm^{-2})$^{-1}$	k_2/(W s cm^{-2})$^{-1}$	k_3/(W s cm^{-2})$^{-1}$	k_4/(W s cm^{-2})$^{-1}$	k_5/(W s cm^{-2})$^{-1}$	z	x	χ^2
SC (SKM)	0.31	—	—	—	0.022	0.80	—	1.05×10^{-3}
SC (UKM)	0.31	0.096	—	—	0.022	0.80	—	4.41×10^{-3}
SC (RKM)	0.35	0.295	0.12	0.05	0.022	0.80	0.325	1.75×10^{-3}
LF^S (SKM)	1.37	—	—	—	0.022	0.95	—	9.26×10^{-3}
LF^S (UKM)	1.37	0.087	—	—	0.022	0.95	—	20.72×10^{-3}
LF^S (RKM)	1.37	1.35	1.1	0.04	0.022	0.95	0.325	4.61×10^{-3}
LF^W (SKM)	374	—	—	—	0.88	1.00	—	15.92×10^{-3}
LF^W (UKM)	374	140	—	—	0.88	1.00	—	8.72×10^{-3}

SC—spin coated, LF^S—Langmuir film polymerized on solid substrate, LF^W—Langmuir film polymerized on water subphase, SKM-simple kinetic model, UKM—unidirectional kinetic model, RKM—reversible kinetic model.

Quantification of the chromatic transition is therefore a central issue with important applicative aspects. In this analysis we consider the integrated intensity of both the excitonic and vibronic peaks after background subtraction and deconvolution of the spectra at each irradiation dose step. We have noted that the sum of the excitonic and vibronic peaks accurately represent the relative fraction of each phase within the films. Previous studies have used only the pair of excitonic peaks (blue and red) for this purpose,[19] while other used the stronger peak from each phase[16,20] or their sum of intensities.[21] In order to obtain the fractions of the blue and red phases throughout the transformation stages, the absorbance signal of each phase after every UV dose increment was normalized by the maximum value of polymer absorbance, as described above.

In order to monitor the chromatic transitions within the film, we have used the unidirectional first order kinetic model (UKM), schematically presented by expression (5):

$$\boldsymbol{M} \xrightarrow{k_1} \boldsymbol{B} \xrightarrow{k_2} \boldsymbol{R} \xrightarrow{k_5} \boldsymbol{D}, \quad \boldsymbol{B} \xrightarrow{k_3} \boldsymbol{D} \tag{5}$$

where the k_1 and k_5 constants correspond to the same phase transitions as in SKM, (expression (1)). The $\boldsymbol{B} \rightarrow \boldsymbol{R}$ transition kinetics is described by the k_2 reaction rate constant, and the degradation process was defined to be allowed either from the blue or the red phases with the same reaction rate, k_5. Thus, the entire polymerization and chromatic transition from the monomer to the blue phase and further to red phase is described using eqn (6)–(9):

$$\frac{\mathrm{d}\boldsymbol{M}}{\mathrm{d}\boldsymbol{H}} = -k_1\boldsymbol{M} \tag{6}$$

$$\frac{\mathrm{d}\boldsymbol{B}}{\mathrm{d}\boldsymbol{H}} = k_1\boldsymbol{M} - k_2\boldsymbol{B} - k_5\boldsymbol{B} \tag{7}$$

$$\frac{\mathrm{d}\boldsymbol{R}}{\mathrm{d}\boldsymbol{H}} = k_2\boldsymbol{B} - k_5\boldsymbol{R} \tag{8}$$

$$\frac{\mathrm{d}\boldsymbol{D}}{\mathrm{d}\boldsymbol{H}} = k_5(\boldsymbol{B} + \boldsymbol{R}) \tag{9}$$

The fit quality parameter (χ^2) was calculated by the formula:

$$\chi^2 = \frac{\sum(x_i - \bar{x}_i)^2}{N - p} \tag{10}$$

where x_i—experimental data, $\bar{x}_i$—calculated data from model equations, N—number of data points and p—number of fit parameters.

The results of the unidirectional kinetic model presented above are also shown in Fig. 4. In these diagrams the measured and calculated relative concentrations of the monomer, polymer with its constituent chromatic phases (blue and red) and degradation phases are compared for the different film types as a function of UV exposure.

The results are plotted on a logarithmic exposure scale (x-axis in Fig. 4) in order to underline the fast kinetics at low exposure doses and demonstrate the three polymerization regions identified in the absorbance curves in Fig. 1 and 2. In region I the monomer phase is dominant and the amount of blue phase is increasing. In LF^W the initial growth of the blue phase occurs in parallel with growth of the red phase due to the fast polymerization rate on water. Region II starts at the maximum content of the blue phase and represents the main stage of the $\boldsymbol{B} \rightarrow \boldsymbol{R}$ transition, where all phases of PDA coexist in the film. And finally, region III begins at the point of equal $\boldsymbol{B}/\boldsymbol{R}$ proportion and includes the completion of the $\boldsymbol{B} \rightarrow \boldsymbol{R}$ transition followed by the degradation of the film material. The shapes of the exposure-resolved curves are basically similar for all films, and all three dynamic regions are present in the same sequence. The kinetic constants obtained by fitting the experimental data to all of the kinetic models for the different films, along with the normalization parameters (z) and fitting quality parameters (χ^2), are summarized in Table 1.

The reaction constant k_2 describes the rate of the chromatic phase transition from the blue to red phase. The k_2 value is high for LF^W film, which results in a fast blue to red transition compared to the low rate of transition in solid supported films. Moreover, according to the unidirectional kinetic model, the k_1/k_2 ratio reflects the stability of the blue phase. In LF^W, this ratio is low and hence manifests the fast $\boldsymbol{B} \rightarrow \boldsymbol{R}$ transition rate, which in turn determines the metastable nature of blue phase and the high ratio of red phase during the irradiation process (Fig. 4c).

We note that unidirectional kinetic model does not depict well the chromatic phase transitions within SC and LF^S film during UV irradiation. The fit quality parameter for LF^S is poor ($\chi^2 = 20.72 \times 10^{-3}$), while for SC film, although the fit quality is reasonable ($\chi^2 = 4.41 \times 10^{-3}$), the model curves do not describe well the chromatic transitions and systematically deviate from the experimental data. The model curves fail to describe the coexistence of the blue and red phases, *e.g.* the plateau region in SC and LF^S films, Fig. 4a and b. Moreover, the relative fraction of the chromatic phases (blue and red) in LF^S according to the model is greater than the actual phase fractions according to the experimental data. Additionally in region II of the irradiation process in SC and LF^S films (Fig. 1b and e) there is little change in the total absorbance intensity despite continuous UV irradiation. Nevertheless, extended UV irradiation induces structural disorder which is manifested in a change in the vibronic/excitonic absorption peak ratio in SC and LF^S samples.[31] Additionally, the experimental data show that there is a shift of the excitonic absorbance peak of the blue phase during UV irradiation. Extended irradiation results in prolonged blue and red phase coexistence during Stage II, suggesting another intermediate phase is actually present between the blue and the red phases, which cannot be resolved independently. On the contrary, the spectral behaviour of LF^W film is different: there is neither a prolonged stage of blue and red phase coexistence (plateau region) nor an absorbance peak shifting during chromatic phase evolution (Fig. 2g and h). Hence, the presence of the intermediate phase is not expected in the LF^W case and the chromatic transition should proceed directly from the blue to red phase.

Reversible kinetic model (RKM). In order to account for the spectral features discussed earlier, and the systematic deviation from the "modelled" UKM kinetics we consider another kinetic model that accounts for the presence of the intermediate phase. The unidirectional kinetic model presented in eqn (5) was modified by the introduction of a reversible state in the blue phase. In the present kinetic model we assume that this phase is an intermediate in the transition to red phase (eqn (11)). According to previous studies,[9,13,16] the chromatic transition from blue to red may progress *via* a reversible intermediate stage, thus the complete expression for the $\boldsymbol{B} \rightarrow \boldsymbol{R}$ transition should be in fact given by ***Blue*** $\leftrightarrow$ ***Intermediate phase*** $\rightarrow$ ***Red***, namely the blue-to-intermediate phase transition is reversible, while the intermediate phase-to-red transition is not.

The reversible kinetic model is given by expression (11):

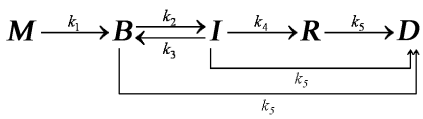

(11)

where the intermediate state is represented by $\boldsymbol{I}$, k_2 kinetic constant describes the rate of the blue to intermediate phase transition, while k_3 constant describes the rate of the reversible reaction from intermediate to blue phase. The irreversible transition from intermediate to red phase is represented by k_4 constant and the degradation process was considered with the same rate from blue, intermediate and red phases with the same constant rate k_5. Hence, the chromatic transition from blue to red *via* intermediate phase takes the form presented in eqn (12)–(16):

$$\frac{d\boldsymbol{M}}{d\boldsymbol{H}} = -k_1\boldsymbol{M} \quad (12)$$

$$\frac{d\boldsymbol{B}}{d\boldsymbol{H}} = k_1\boldsymbol{M} - k_2\boldsymbol{B} - k_5\boldsymbol{B} + k_3\boldsymbol{I} \quad (13)$$

$$\frac{d\boldsymbol{I}}{d\boldsymbol{H}} = k_2\boldsymbol{B} - k_3\boldsymbol{I} - k_5\boldsymbol{I} - k_4\boldsymbol{I} \quad (14)$$

$$\frac{d\boldsymbol{R}}{d\boldsymbol{H}} = k_4\boldsymbol{I} - k_5\boldsymbol{R} \quad (15)$$

$$\frac{d\boldsymbol{D}}{d\boldsymbol{H}} = k_5(\boldsymbol{B} + \boldsymbol{I} + \boldsymbol{R}) \quad (16)$$

Eqn (6)–(9) and (12)–(16) are consistent with eqn (2)–(4), by setting $\boldsymbol{P} = \boldsymbol{B} + \boldsymbol{R}$ in case of UKM or $\boldsymbol{P} = \boldsymbol{B} + \boldsymbol{I} + \boldsymbol{R}$ in case of the RKM. The full solution of the unidirectional and reversible PDA kinetics model is provided in the ESI.†

Fig. 3 gives a structural evidence for a phase transformation into an intermediate phase. It shows that the triple bond of the

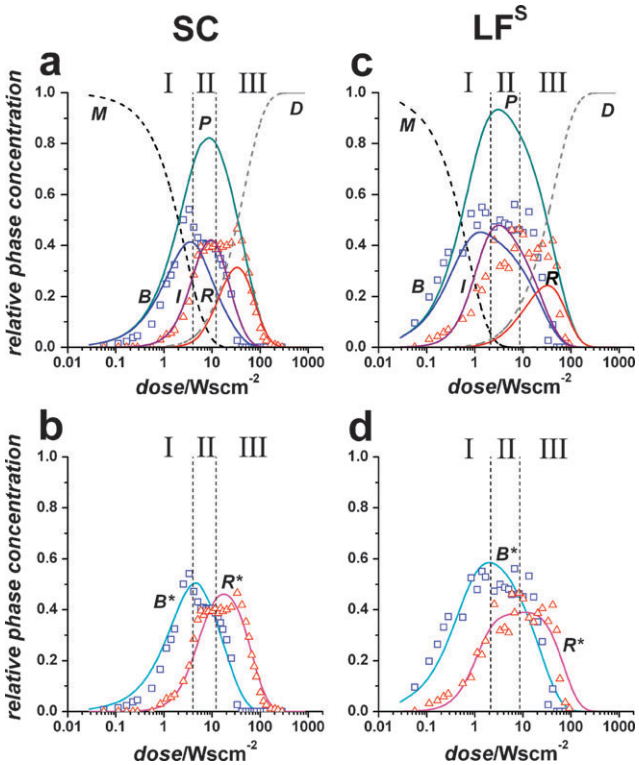

Fig. 5 Exposure-resolved plots calculated from reversible kinetic model (eqn (11)) depicting the phase transitions of PDA for (a, b) SC and (c, d) LF^S films. The empty squares and triangles represent experimental data for the blue and red phases, respectively. The fitting solid lines calculated from reversible kinetic model eqn (12)–(16) allowed us to estimate the values of the kinetic constants, $k_1 - k_5$. The (***B***), (***I***) and (***R***) solid lines represent calculated relative phase concentration of pure chromatic phases, while (***B****) and (***R****) solid lines represent total blue and red absorbance signals, respectively, calculated with expression (17) by using the distribution parameter, *x*.

blue phase at 2101 cm^{-1} is shifting under UV irradiation to 2077 cm^{-1}. The peak position as function of UV dose is displayed in Fig. 3b, showing that this shift occurs at 1–10 W s cm^{-2}, and coincides with the growth of an intermediate phase at these doses, as obtained from the kinetic model, Fig. 5 below. We note that the red phase shows a triple bond at 2120 cm^{-1} (with the 633 nm excitation); hence the 2077 cm^{-1} line is not related to the red phase. In the inset we show data obtained without UV, *i.e.* the polymerization proceeds by a two-photon process[10] of the 788 nm laser used for the Raman study. In this case we were able to resolve the coexistence of two peaks, *i.e.* the peak does not just shift position with the UV dose. This shows that the intermediate phase coexists with the blue phase, and further supports our claim that there is a phase transformation into a distinct intermediate phase.

The transformation from the blue phase to red involves the formation of a smaller and more condensed unit cell. The cell shrinkage is caused by reducing the distance between adjacent polymer chains from 4.83 Å in the blue to 3.9 Å in the red phase, a 20% reduction. That in turn drives the alkyl chains into a more upright position and, as a result, to its stable phase.[15] Thus we consider that there is no reversible reaction back from the red phase. On the other hand, the Raman data for the intermediate phase shows that only the triple bond is slightly shifted (Fig. 3), suggesting that some rearrangement of the conjugated backbone take place prior to the transition to the red phase. Structurally, the intermediate phase is related to the blue and therefore the $\boldsymbol{B} \rightarrow \boldsymbol{I}$ transition is expected to be reversible.

According to previous studies,[9,13,16] absorbance peaks of the intermediate phase are expected to overlap with the vibronic peak of the blue phase and excitonic peak of the red phase (*ca.* 600 and 550 nm, respectively). Due to this overlapping, the presence of the intermediate stage cannot be proven directly, hence the proposed mechanism and consequent reversible kinetic model are in fact indirect support of such a scenario. Yet, it is interesting to note that it was the only way we found to describe the transition kinetics more accurately. According to our best fit, the reversible kinetic model depicts in an optimal way the phase transitions in SC and LF^S films, while the unidirectional kinetic model depicts it for the LF^W film. Note that the same kinetic constants as the best fit for LF^W were obtained by both reversible and unidirectional kinetic models. Since blue and red absorbance signals include absorbance of the intermediate phase, in order to express the experimental absorbance signal we used an additional parameter, x, which describes the distribution of the intermediate phase fraction among the blue and red absorbance signals. Signals associated with blue and red phases, according to the reversible kinetic model, can be in fact described by the following expression:

$$\begin{aligned} \text{Blue absorbance } (B^*) &= B + x \cdot I \\ \text{Red absorbance } (R^*) &= R + (1 - x) \cdot I \end{aligned} \qquad (17)$$

where $\boldsymbol{B}$, $\boldsymbol{I}$ and $\boldsymbol{R}$ are pure blue, intermediate and red phase fractions calculated from the reversible kinetic model.

The reaction constant k_2 describes the rate of the chromatic phase transition from the blue to intermediate phase. For SC and LF^S films this rate is slow, compared to the fast blue to red phase transformation in the LF^W film. Due to this fact, the stability of the blue phase on solid supported PDA films is greater than on the air–water interface. The k_3/k_2 ratio describes the degree of reversibility between blue and intermediate phase. In LF^S films the degree of reversibility is greater than in SC films, thus the blue phase is more stable during UV irradiation in case of LF^S (Fig. 5a and b *vs.* c and d). This finding can also be observed from the experimental results, where the pure red phase exists only at high doses of irradiation, just before the final degradation of the film (Fig. 1f). In the case of SC, the stability of the blue phase is lower, thus the red phase is better separated from the blue phase in the kinetics diagram compared to LF^S (Fig. 5). The stability of the blue phase can also be explained by means of k_4/k_3 ratio. As this ratio is higher the faster is the transition from intermediate to red phase. For LF^S this ratio is lower than for SC, therefore the blue phase is more dominant in the exposure-resolved diagram. The reversible intermediate phase is more intense in LF^S than in the SC film, consequently the blue phase signal is more dominant then a red one throughout all of the irradiation period. Note, the distribution parameter (x), which was obtained as the best fit, for the intermediate phase is equal for both SC and LF^S films.

According to eqn (5) & (11) the degradation process was defined to be allowed to occur from all the chromatic phases of PDA with the same reaction rate, k_5. For solid supported films the degradation process occurs from all of the chromatic PDA phases, whereas in LF^W this process occurs mainly from the red phase, due to the greater value of k_2 compared to the k_5 constant.

It is interesting to note that the good quality of fit (low χ^2 values) for SKM model are significantly poorer for UKM, but considerably better for RKM. An attempt to resolve blue to red transition using UKM decreases the quality of the fit, but when RKM is used the quality of the fit rises back to the values obtained in the SKM case. This behaviour supports the necessity and significance of the RKM when chromatic transitions are resolved in polydiacetylene solid supported films.

Conclusion

In this work we have monitored and analyzed the phase transition kinetics for thin polydiacetylene films prepared by spin coating and Langmuir techniques, which were polymerized either on a solid support or directly at an air–water interface. The radiation-induced phase transitions: from the colorless monomer, *via* the metastable blue phase, to the red polydiacetylene phase, and finally to degradation of the material, were fitted using different kinetic transition models. The simple kinetic model was applied for the basic polymerization reaction ($\boldsymbol{M} \rightarrow \boldsymbol{P} \rightarrow \boldsymbol{D}$), while chromatic phase transitions within the polymer were described by the unidirectional and the reversible kinetic models. In UKM, a unidirectional transition from the blue to red phase was assumed, while in RKM the blue to red transition was proposed to progress *via* an intermediate and reversible stage. The phase transition process for LF^W films

was successfully modelled by UKM, while in case of SC and LF^S films only RKM is consistent with the phase transformations, which is an indirect proof of an intermediate phase, separating the blue and red phases. Raman data, showing a shift of the triple bond frequency, is a support for the presence of this additional phase. Exposure-resolved diagrams, obtained by deconvolution of background-subtracted absorbance curves, allowed evaluation of the kinetic constants for all phase transitions. Polymerization and phase transformation kinetics of molecularly thick PDA films floating freely on the air–water interface (Langmuir trilayer films) are two orders of magnitude faster compared to PDA Langmuir trilayer films polymerized on solid substrate and three orders faster compared to spin-coated films of the same material. Moreover, the blue phase of PDA is more stable under UV irradiation in solid support films, compared to those which were polymerized directly at the air–water interface.

Experimental

Chemicals

10,12-Pentacosadiynoic acid ($CH_3(CH_2)_{11}C{\equiv}C{-}C{\equiv}C(CH_2)_8$-COOH; PCDA) ($\geq$ 97% HPLC grade, Fluka), chloroform stabilized with amylene (HPLC grade, Bio Lab, Ltd., Israel) were used as received. Distilled water was obtained using a Millipore filtration system with a resistivity of 18.2 MΩ cm.

Langmuir film (LF) preparation

PCDA (2 mM in chloroform) was carefully spread onto the distilled water surface on a Nima (Coventry, UK) Langmuir trough (Model 611). The film was held for at least 15 min at zero pressure prior to compression to allow for solvent evaporation, and was then compressed at a rate of 10 cm^2 min^{-1} until a surface pressure of 25 mN m^{-1} was reached. During compression, the film undergoes a monolayer-to-trilayer transition, and in its final stable condition of three molecular layers reaches a thickness of $\sim$9 nm.[14,32] In case of LF^W, following compression, UV irradiation of the compressed films were performed with a UV lamp (254 nm, 6 W) from a distance of 8 cm above the air–water interface, corresponding to an irradiation power density of 1.1×10^{-4} W cm^{-2} on the floating PDA film. For the optical absorbance measurements the films were deposited on a pre-cleaned glass substrate by the Langmuir–Schäffer (LS) technique. In case of LF^S, the unpolymerized films were transferred onto solid support using the LS or Langmuir – Blodgett (LB) methods. In LB deposition the films were vertically raised onto quartz substrates using a dipper device, while in LS deposition the films were horizontally lifted from the air–water interface onto quartz substrates. A Pen-ray® UV lamp (254 nm, 24 W) at a distance of 1 cm was used for irradiation, corresponding to an irradiation power density of 2.8×10^{-2} W cm^{-2}.

Spin-coated film preparation

A solution of 6.72 mM PCDA in chloroform was carefully applied onto a pre-cleaned quartz substrate. A standard spin coating instrument (Lawrell WS-400A-6NPP/lite) was operated at a speed of 2000 rpm for 2 min, resulting in a 40–50 nm thick film. For the spin-coated films, UV irradiation was performed using pen-ray® UV lamp (254 nm, 24 W) from a distance of 1 cm, corresponding to an irradiation power density of 2.8×10^{-2} W cm^{-2}.

Optical absorbance measurements

Optical absorbance measurements were carried out on a TRIAX 320 (Jobin Yvon-Spex) spectrophotometer equipped with a white light source (150 W tungsten-halogen lamp) and CCD detector, and on a Jasco V-550 spectrophotometer equipped with a double beam system with a single monochromator, halogen lamps and photomultiplier detector. For LF^S and SC films the optical absorbance measurements were done *in situ* during the polymerization process: *i.e.* after the PDA was deposited on quartz substrate the optical absorbance was measured at the same position on the film after each increment of UV exposure. On the other hand, optical absorbance measurements of LF^W required a series of samples that were polymerized directly on the water surface using progressive increments of UV radiation. It is important to note that in a series of control experiments we have ruled out any significant contribution of the 150 W tungsten–halogen lamp to the phase transition process.

Raman characterization

Raman spectra were collected using a Jobin-Yvon (JY) LabRam HR 800 micro-Raman system, equipped with a liquid-N_2-cooled detector. Excitations were with a 633 nm He–Ne laser and a 788 nm NIR diode laser through a 50× microscope objective lens. The power on the sample was attenuated using neutral-density (ND) filters. Most measurements were taken using a 600 grooves/mm grating and a microscope confocal hole setting of 100 μm giving a resolution of about 4 cm^{-1}.

Acknowledgements

Support from the German–Israeli Foundation for Scientific Research and Development (GIF) (grant G-791-133.10/2003) is gratefully acknowledged. We thank Ayelet Vilan for significant help during the early stages of this work.

References

1 S. Okada, S. Peng, W. Spevak and D. Charych, *Acc. Chem. Res.*, 1998, **31**, 229–239.
2 J.-M. Kim, Y. B. Lee, D. H. Yang, J.-S. Lee, G. S. Lee and D. J. Ahn, *J. Am. Chem. Soc.*, 2005, **127**, 17580–17581.
3 Y.-I. Su, *J. Colloid Interface Sci.*, 2005, **292**, 271–276.
4 Y. Yang, Y. Lu, M. Lu, J. Huang, R. Haddad, G. Xomeritakis, N. Liu, A. P. Malanoski, D. Sturmayr, H. Fan, D. Y. Sasaki, R. A. Assink, J. A. Shelnutt, F. V. Swol, G. P. Lopez, A. R. Burns and C. J. Brinker, *J. Am. Chem. Soc.*, 2003, **125**, 1269–1277.
5 N. G. Semaltianos, H. Araujo and E. G. Wilson, *Surf. Sci.*, 2000, **460**, 182–189.
6 J. P. Fouassier, B. Tieke and G. Wegner, *Isr. J. Chem.*, 1979, **18**, 227–232.
7 Y. Tokura, K. Ishikawa, T. Kanetake and T. Koda, *Phys. Rev. B: Condens. Matter*, 1987, **36**(5), 2913.
8 W. Wensel and G. H. Atkinson, *J. Am. Chem. Soc.*, 1989, **111**, 6123–6127.
9 M. Schott, *J. Phys. Chem. B*, 2006, **110**, 15864–15868.

10 O. Shusterman, A. Berman, Y. Golan, B. Horovitz and L. Zeiri, *J. Phys. Chem. B*, 2009, **113**, 1273–1276.
11 D. Charych, J. D. Nagy, W. Spevak and M. Bednarski, *Science*, 1993, **261**, 585–588.
12 R. W. Carpick, D. Y. Sasaki and A. R. Burns, *Langmuir*, 2000, **16**, 1270–1278.
13 R. W. Carpick, D. Y. Sasaki, M. S. Marcus, M. A. Eriksson and A. R. Burns, *J. Phys.: Condens. Matter*, 2004, **16**, R679–R697.
14 D. Y. Sasaki, R. W. Carpick and A. R. Burns, *J. Colloid Interface Sci.*, 2000, **229**, 490–496.
15 Y. Lifshitz, Y. Golan, O. Konovalov and A. Berman, *Langmuir*, 2009, **25**, 4469–4477.
16 A. Deckert, J. Home, B. Valentine, L. Kernan and L. Fallon, *Langmuir*, 1995, **11**, 643–649.
17 X. Huang, S. Jiang and M. Liu, *J. Phys. Chem. B*, 2005, **109**, 114–119.
18 J. Song, J. S. Cisar and C. R. Bertozzi, *J. Am. Chem. Soc.*, 2004, **126**, 8459–8465.
19 U. G. Hofmann and J. Peltonen, *Langmuir*, 2001, **17**, 1518–1524.
20 Z. Huilin, L. Weixing, Y. Shufang and H. Pingsheng, *Langmuir*, 2000, **16**, 2797–2801.
21 D. W. Britt, U. G. Hofmann, D. Mobius and S. W. Hell, *Langmuir*, 2001, **17**, 3757–3765.
22 D. J. Ahn, S. Lee and J.-M. Kim, *Adv. Funct. Mater.*, 2009, **19**, 1483–1496.
23 M. A. Reppy and B. A. Pindzola, *Chem. Commun.*, 2007, 4317–4338.
24 E. Geiger, P. Hug and B. A. Keller, *Macromol. Chem. Phys.*, 2002, **203**, 2422–2431.
25 R. Jelinek, *Drug Dev. Res.*, 2000, **50**, 497–501.
26 A. Lio, A. Reichert, D.-J. Ahn, J. O. Nagy, M. Salmeron and D. H. Charych, *Langmuir*, 1997, **13**, 6524–6532.
27 A. S. Alekseev, T. Viitala, I. N. Domnin, I. M. Koshkina, A. A. Nikitenko and J. Peltonen, *Langmuir*, 2000, **16**, 3337–3344.
28 D. Bloor and M. R. Worboys, *J. Mater. Chem.*, 1998, **8**(4), 903–912.
29 K. Itoh, T. Nishizawa, J. Yamagata, M. Fujii, N. Osaka and I. J. Kudryashov, *J. Phys. B: At., Mol. Opt. Phys.*, 2005, **109**, 264–270.
30 Y. Lifshitz, A. Upcher, A. Kovalev, D. Wainstein, A. Rashkovsky, A. Berman and Y. Golan, in preparation, 2010.
31 J. I. Bredas, K. Cornil, F. Meyers and D. Beljone, in *Handbook of Conducting Polymers*, ed. T. A. Skotheim, R. L. Elsenbaumer and J. R. Reynolds, Marcel Dekker Inc., New York, 2nd edn, 1998, ch. 1, pp. 1–25.
32 A. Berman and D. Charych, *J. Cryst. Growth*, 1999, **198–199**, 796–801.

